

MPDNet: Multimodal Pneumonia Detection Network Simulating Clinical Diagnosis Process

Qiuli Wang, Zhihuan Li, Dan Yang, Chen Liu*, Xiaohong Zhang*

Abstract—Objective: Pneumonia detection is one of the most crucial steps in pneumonia diagnosing system. Clinical information of patients plays an important role in detection of pneumonia. In this paper, a Multimodal Pneumonia Detection Network(MPDNet) is described for clinical pneumonia detection. **Method:** MPDNet is based on deep learning neural network and analyzes multimodal data: three-channel CT images, patient chief complaints, patient age and gender. Original CT images are one-channel grey level images. In MPDNet, each slice of CT is transformed into one three-channel(Lung Window, High Attenuation, Low Attenuation) image, different channel can provide different information of lung density and become supplements to each other. Visual features from three-channel images are qualitative information for pneumonia detection. Patient chief complaints provide information about lesion location, symptoms or how long patients have been ill. Chief complaints are related to CT images and enhance information extracted from CT images. Information about age and gender can provide priori information for decision making process. CT visual features, complaint semantic features, patient age and gender will be fused together and calculate joint distribution to predict whether these cases are pneumonic. We use Recurrent CNN, which can keep 3D spatial information and reduce the need of calculation resource, to capture visual features from CT image data. A Long Short Term Memory(LSTM) network is used to analyze semantic features of patient chief complaints. **Results:** We analyze 1002 clinical cases from The First Affiliated Hospital of Army Medical University. Our model achieves 0.945 in accuracy, and has a very balanced performance in sensitivity and specificity. As far as we know, we are the first to detect pneumonic cases using large scale clinical multimodal data. **Conclusion:** Our method proves that multimodal data provides more abundant information than image data only and get very convincing results. **Significance:** Making decision based on multimodal data conforms clinical practice. Our model can be extended and include more multimodal clinical data to give out more reliable and explainable detection results.

Index Terms—Multimodal Data, Pneumonia Detection, Computed tomography (CT), Computer-aided detection and diagnosis (CAD)

I. INTRODUCTION

PNEUMONIA is a very common thoracic disease in daily life. In clinical practice, a radiologist needs to consider

different source of information to decide on the next treatment plan, as a result, multimodal data plays the key role in decision making process. According to the survey, a radiologist of a major hospital need to diagnosis hundreds of pneumonia cases every day. Thus, developing a fast, robust and accurate CAD system to perform automated detection of pneumonia is meaningful and important.

There have been several methods and epidemiological studies for pneumonia detection, monitoring and diagnosing like [1]–[3]. Hoo-Chang Shin [1] combined CNN and LSTM [4], proposed a method which could describe the contexts of a detected diseases based on the deep CNN features. This method used CNN to extract features from chest X-Ray and used LSTM to generated MeSH [5] terms for chest X-Ray. In 2017, Xiaosong Wang et al. [6] provided hospital-scale chest X-ray database ChestX-ray8 which contained eight common thoracic diseases. This database allowed researchers use deeper neural network to analyze thoracic diseases. They tested different pre-trained CNN models on this dataset. Experiments showed that ResNet50 achieved highest AUROC score 0.6333 in classifying pneumonia. They also provided ChestX-ray14 which contains more kinds of thoracic diseases. Based on this database, later in 2017, Yao et al. [7] achieved 0.713 in AUROC score using DenseNet Image Encoder. Pranav Rajpurkar, Andrew Y. Ng et al. [8] developed CheXnet with 121 convolutional layers and achieved AUROC 0.7680 in pneumonia classification. In 2018, Xiaosong Wang et al. [9] proposed TieNet, which could classify the chest X-Rays into different diseases and generate the report at the same time. In TieNet, CNN was used capture features of chest X-Rays, RNN learned these features and generated report based on attention mechanism, which could help model to focus on different parts of chest X-Ray alone with the generation of reports. In pneumonia classification problem, they achieved 0.947 in AUROC based on report, but they only achieved 0.917 in AUROC on hand-labeled data.

Studies above have something in common. First of all, they are designed for chest X-Rays. Chest X-rays used to be the best available method for detect pneumonia, played a crucial role in clinical care and epidemiological studies [10], [11]. However, compared to chest X-rays, CT scans have a clearer view of patients' bodies, since bones, skin, vessels, mediastinal and lung tissues may cause overlapping shadows in chest X-ray and cause misdiagnosis. CT allows visualization of lung structures [12], which can help to diagnosis pneumonia in early stage and avoid delayed treatments. Each slice of CT scans is a 2D image of human body scan, besides 2D visual features from CT, you can also reconstruct 3D structure of

Q. Wang, Z. Li, D. Yang are with the School of Big Data & Software Engineering, Chongqing University, Chongqing 401331, China. E-mail: wangqiuli@cqu.edu.cn, 201724131013@cqu.edu.cn, dyang@cqu.edu.cn.

X. Zhang is with the Key Laboratory of Dependable Service Computing in Cyber Physical Society, Ministry of Education, Chongqing University, Chongqing 400044, China, also with the School of Software Engineering, Chongqing University, Chongqing 401331, China, and also with the State Key Laboratory of Coal Mine Disaster Dynamics and Control, Chongqing University, Chongqing 400044, China. E-mail: xhongz@cqu.edu.cn.

L. Chen is with the Radiology Department, The First Affiliated Hospital of Army Medical University, 400032, Chongqing, China. E-mail: cqliuchen@foxmail.com.

human bodies using these slices. Extensive studies show that 3D CNN is the best choice for keeping 3D spatial information in CT [13]. However, 3D CNN cannot be applied to raw CT data directly since it will bring a heavy burden to computers. Radiologists need to accurately measure the lesions, so we cannot reduce the size of images by resizing at will.

Second, these models are not designed following the radiologists' diagnosing process but are designed for the convenience of computer vision studies and deep learning model training. For models like CheXnet, image information is the key of models. Few of them combine image visual features with clinical information. Models like TieNet do combine image visual features with descriptions about images written by radiologists. We believe using descriptions about images written by radiologists to improve models is not quite convincing, since descriptions like 'Findings' and 'impressions' sometimes include diagnosis conclusions. However, there have been many studies try to analyze multimodal data like [14], [15]. Multimodal data can be multimodal images [16] or multimodal data source. Patients' chief complaints is a very useful information when doctors are making decisions [17], since chief complaints is patients' direct feeling about their physical condition, telling us the patients' pain location, symptoms and how long have they been ill. Moreover, information of age and gender can provide priori information [18], [19]. However, as far as we know, few studies use this information to improve CAD systems for pneumonia.

In general, there are two major drawbacks of existing CAD systems for pneumonia: (1) They cannot handle raw CT scans, which allows visualization of lung structures; (2) Few studies consider multimodal clinical information like patients' chief complaints, which is conflict to clinical practice.

To address such drawbacks, we propose a novel Multimodal Pneumonia Detection Network(MPDNet) for clinical pneumonia detection. The architecture of MPDNet is shown in Fig 1. We use raw data collected from The First Affiliated Hospital of Army Medical University, each case contains not only CT image information, but also clinical information about patient gender, age and chief complaint. Herein, (i) each CT image will be transformed into a 3-channel image with three windows: Lung Window(LW), High Attenuation(HA) and Low Attenuation(LA). LW provides visual features of normal lung tissues, HA provides visual features of abnormal increase in lung density, LA provides visual features of abnormal decrease in lung density. Three channels complement each other, which not only maintains the ability to extract information from normal lung tissues, but also increases the ability to extract information from abnormal lung tissues. (ii) We also include clinical data in our MPDNet. Chief complaints can provide location of pain, symptoms and how long have patients been ill. These information is related to CT image and enhance the visual features extracted from CT. (iii) Information about age and gender can provide priori information since patients of different age and gender have differences in the morphology of thoracic cavity and lungs. (iv) In order to reduce the burden of calculation, we treat CT slices as short video frames and a Recurrent Convolutional Neural Network(RCNN) is used to capture visual features from CT slices. RCNN uses a 2D

CNN to capture visual features from each 2D slice, and LSTM captures relationships between slices. We use another LSTM to analyze semantics from chief complaints. Information of age and gender will be treated as two extra variables. Our model MPDNet, as shown in Fig 1, will learn a joint distribution of all features above and gives out the final results.

The remainder of the manuscript is organized as follows. Section II describes the prepare of dataset and pre-process steps. Section III describes the architecture of MPDNet and details of our model. Section IV reports our experimental results. We further discusses some key points of proposed model and some phenomenons shown during experiments in this section. Our conclusions are summarized in section V.

II. DATASET PROCESSING

A. CT Image Data and Multimodal Data Generation

Because of the shortage of public available CT dataset for pneumonia, we use raw data from the Radiology Department of The First Affiliated Hospital of Army Medical University. We get 1036 cases of CT(842 pneumonic cases, 464 healthy cases) from hospital PACS(Picture Archiving and Communication Systems). Raw data from hospital may have more than one series of images and each series has specific data type, image windows, or different angles. Generally speaking, radiologists and doctors will use series under lung window with smallest 'Slice Thickness', but for deep learning models, each case can only have one series. We design a protocol to pick up specific series for us.

First of all, we eliminate these cases which start scanning from the middle of the chest. Then we pick up the best series from the whole cases according to the following requirements:

(a) We choose the series with the specific 'Convolution Kernel'. Different 'Convolution Kernel' may have different data types or different image windows, as shown in Fig 2. We need to notice that these names of 'Convolution Kernel' vary between hospitals and CT equipments, so if you want to adopt this protocol, you need to observe 'Convolution Kernel' in your environment. In our study, we choose 'B31f', 'I31f 3', 'B70f', 'B80f', 'B70s'. Number of different 'Convolution Kernel' is shown in Fig 3.

(b) We remove series like 'Patient Protocol', 'Topogram'. These series, as shown in Fig 2, contain some basic parameters and information about CT equipments.

(c) We calculate 'Slice Thickness' of each series, and keep series with the smallest 'Slice Thickness', since small thickness may keep more detailed information of body structure.

(d) If there were more than one series meet the last two requirements, we will keep the series with the largest number of slices, which can have a larger span of view.

As a result, 552 pneumonic cases and 450 cases of healthy people (1002 cases total) are left. Dataset is divided into training/validation/testing as 60% / 20% / 20% and make them identically distributed in three parts of datasets, so we have 602 cases in training set, 200 cases in validation set, 200 cases in test set. Number of healthy and pneumonic cases in different slice-thickness is shown in Table I. Each CT scan has a case file. In case files, we can get patient basic information: patient ID, gender, age and complaint.

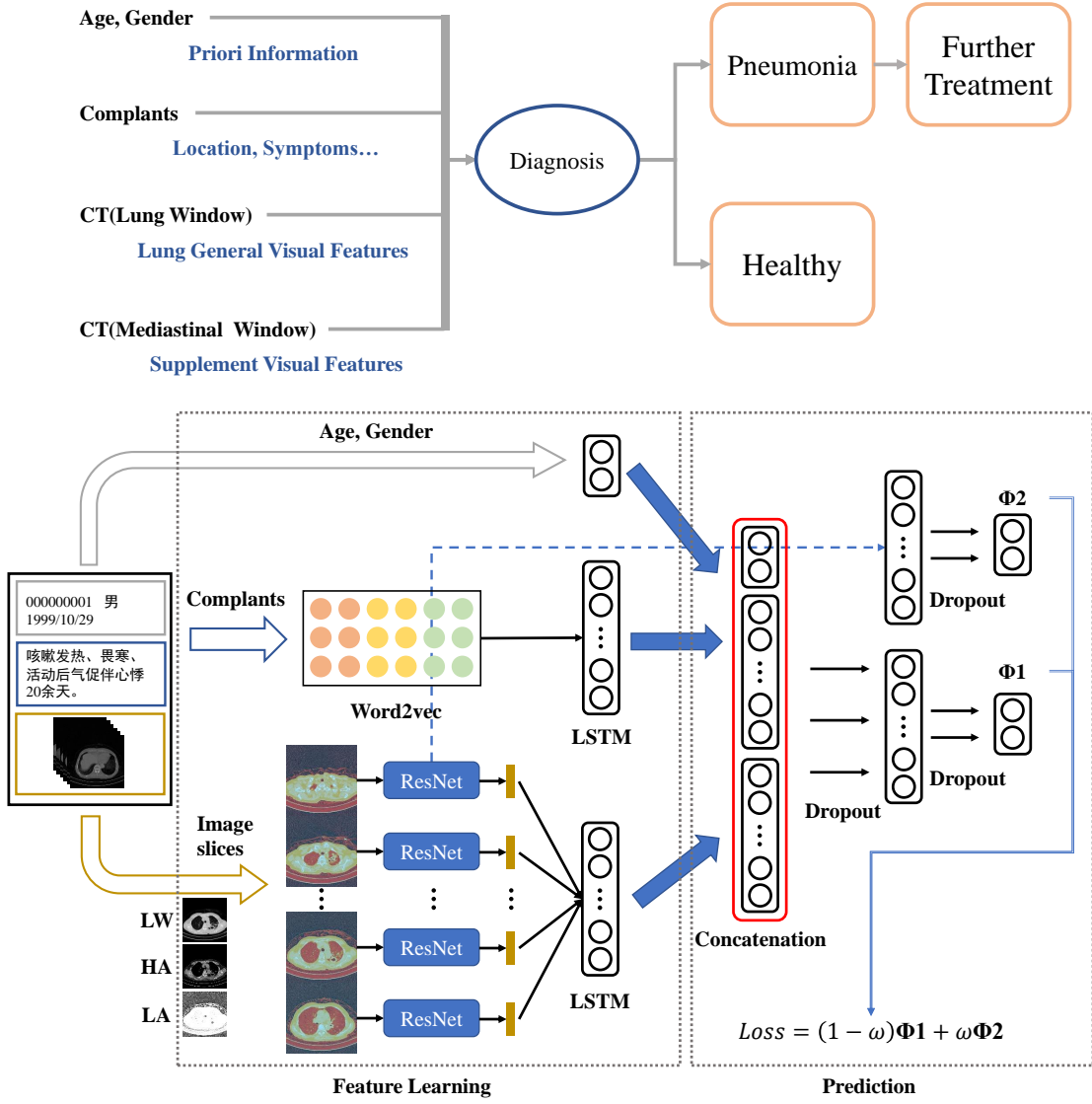


Fig. 1. Architecture of MPDNet. In this figure, sub-figure above is clinical practice of detecting pneumonia. Age and gender provide priori information, complaints provide information like symptoms, location of pain, different CT windows provide visual features. Sub-figure below is MPDNet. The black rectangle contains raw information from hospital. Information in grey rectangle is about age and gender, information in blue rectangle is complaints, information in yellow is CT image data. Chief complaints will be transformed into matrices by Word2vec and analyze by one LSTM network. Image will be fed into RCNN. LW, HA, LA represent three image window: lung window, high attenuation window and low attenuation window. Age and gender will be treated as two additional features. These three kinds of information will be concatenated in red rectangle and fed into fully-connected layers to get prediction

TABLE I
NUMBER OF HEALTHY AND PNEUMONIC CASES IN DIFFERENT
SLICE-THICKNESS

Slice-Thickness	Healthy	Pneumonic
1 mm	0	24
1.5 mm	1	7
2 mm	444	386
3 mm	0	127
5 mm	5	8
Total	450	552

1) *Pre-processing of CT Image Data:* There are different kinds of image windows for CT reader, such as windows for bone, brain, chest or lung. Images under different im-

age windows will highlight different tissues of bodies. As mentioned in section II-A1, we can see that each series of CT actually has one specific 'Convolution Kernel'. But it may make data inconsistent between different cases. So we transform raw data into HU(Hounsfield Unit) values. The Hounsfield Unit is a quantitative scale for describing radio-density. After transformed into HU value matrices, all slices from CT scans will have the same unit of measure.

Following the study in [20] [21], HU value matrices will be transformed into images using three HU windows: Lung Window(LW) [-1000, 400HU], High Attenuation(HA) [-160, 240HU], Low Attenuation(LA) [-1400, -950HU]. For each slice, it will generate three one-channel grey level images(LW, HA, LA). Then we compress three one-channel grey level images into one three-channel false color RGB image. The

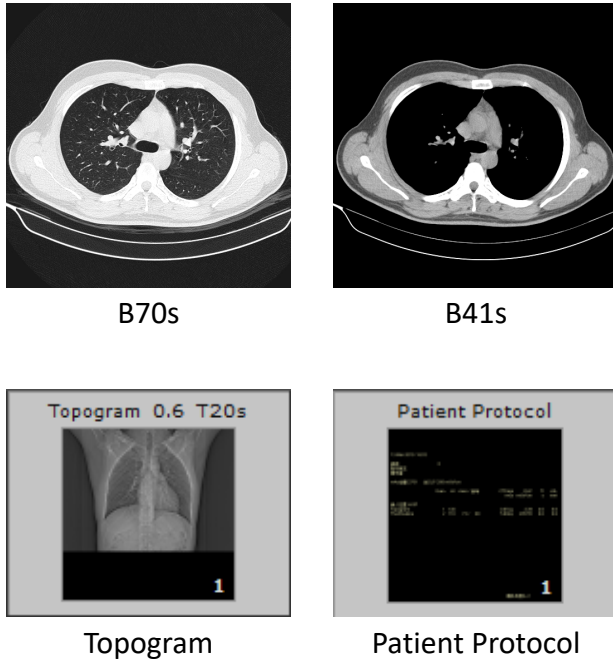


Fig. 2. Scans under Different ‘Convolutional Kernel’. Slice under ‘B70s’ has clearer view of lungs, slice under ‘B41s’ has clearer view of heart. ‘Patient Protocol’ and ‘Topogram’ contain some basic parameters of CT equipments or information about radiologists, which are not suitable for CNN.

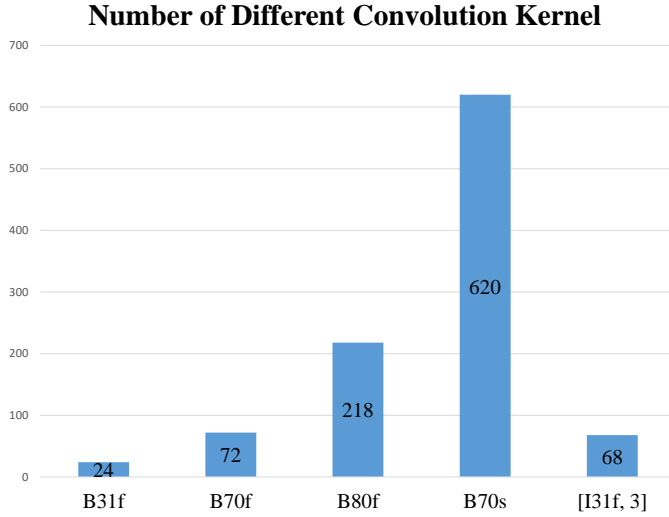


Fig. 3. Number of Different ‘Convolution Kernel’. We notice that in the Radiology Department of The First Affiliated Hospital of Army Medical University, ‘B70s’ is the most common parameter used in clinical. However, this parameter varies between hospitals and clinics.

‘Slice Thickness’ between each slice is adjusted into 10mm, and each case will keep 32 slices.

As shown in Fig 4, we can clearly see that three-channel images can show more density information about lung tissues. Original CT images are actually grey level images, high dense tissues are white, normal lung tissues and low dense tissues are tend to be black. Three-channel false color images have a larger scale of colors. First of all, high dense tissues will

still tend to be white, like bones, high dense tissues in lungs. Second, normal lung tissues will tend to be red, low dense tissues tend to be black, which is very useful when patients have severe lung diseases. The influence of different HU value ranges will be discussed in section IV-B.

2) *Pre-processing of Patient Age, Gender and Chief Complaints*: The pre-process steps of age, gender and chief complaints is shown in Fig 5. Information about age and gender will be transformed into a two-dimensional array. For example, patient in Fig 5 is an adult male, who was born in 1999-10-29. His gender and age will be transformed to $[1, 20]$. A female patient born in 1993 will have $[0, 26]$ to represent her information. 1 represents male patient, 0 represents female patient.

For patients’ chief complaints, since all chief complaints are written in Chinese, we have to do Chinese word segmentation. Chinese word segmentation is a very difficult problem so we will take a short cut and use a mature tools: Jieba text segmentation¹ to segment Chinese sentences into Chinese word sequences. An example of Chinese word segmentation is shown in green rectangle in Fig 5. After word segmentation, we use word2vec [22] [23] to embed word sequences into vectors and use CBOW(Continuous Bag-of-Words) to capture relationship between words. Since our corpus is very small, the embedding size is 50, and window size for CBOW is 3. We set length of Chinese word sequence to 16 since 16 is the maximum length among all chief complaint sequences. For those sequences whose length is less than 16, we add ‘None’ to fill up the voids and increas length to 16. The details of word2vec will not be discussed here. After embedding, each word will be embedded into a vector of 50 dimensions.

III. MULTIMODAL PNEUMONIA DETECTION NETWORK

A. Construction of RCNN

RCNN(Recurrent Convolutional Neural Network) has been proved to be very useful in video caption, description and classification [24] [25], some studies have applied RCNN to medical image analyze. Zreik, Majd et al. [26] recently used RCNN for automatic detection and classification of coronary artery plaque, they used CNN extracts features out of $25 \times 25 \times 25$ voxels cubes, and used an RNN to process the entire sequence using gated recurrent units (GRUs) [27]. KL Tseng et al. [28] exploited convolutional LSTM to model a sequence of 2D slices, and jointly learn the multi-modalities and convolutional LSTM in an end-to-end manner to segment 3D biomedical images.

As mentioned in section I, CT allows visualization of lung structures, which brings a large amount of redundant information, like muscle, vessels and bones. It will cost lots of calculation resource if we use 3D CNN directly. However, if we treat CT slices as short video frames, we can analyze them using RCNN. In RCNN, each slice will be fed into CNN in sequence and get a sequence of visual features. Then this sequence of features will be fed into RNN, so that we can reduce the need of calculation resource and keep 3D spatial

¹<https://github.com/fxsjy/jieba>

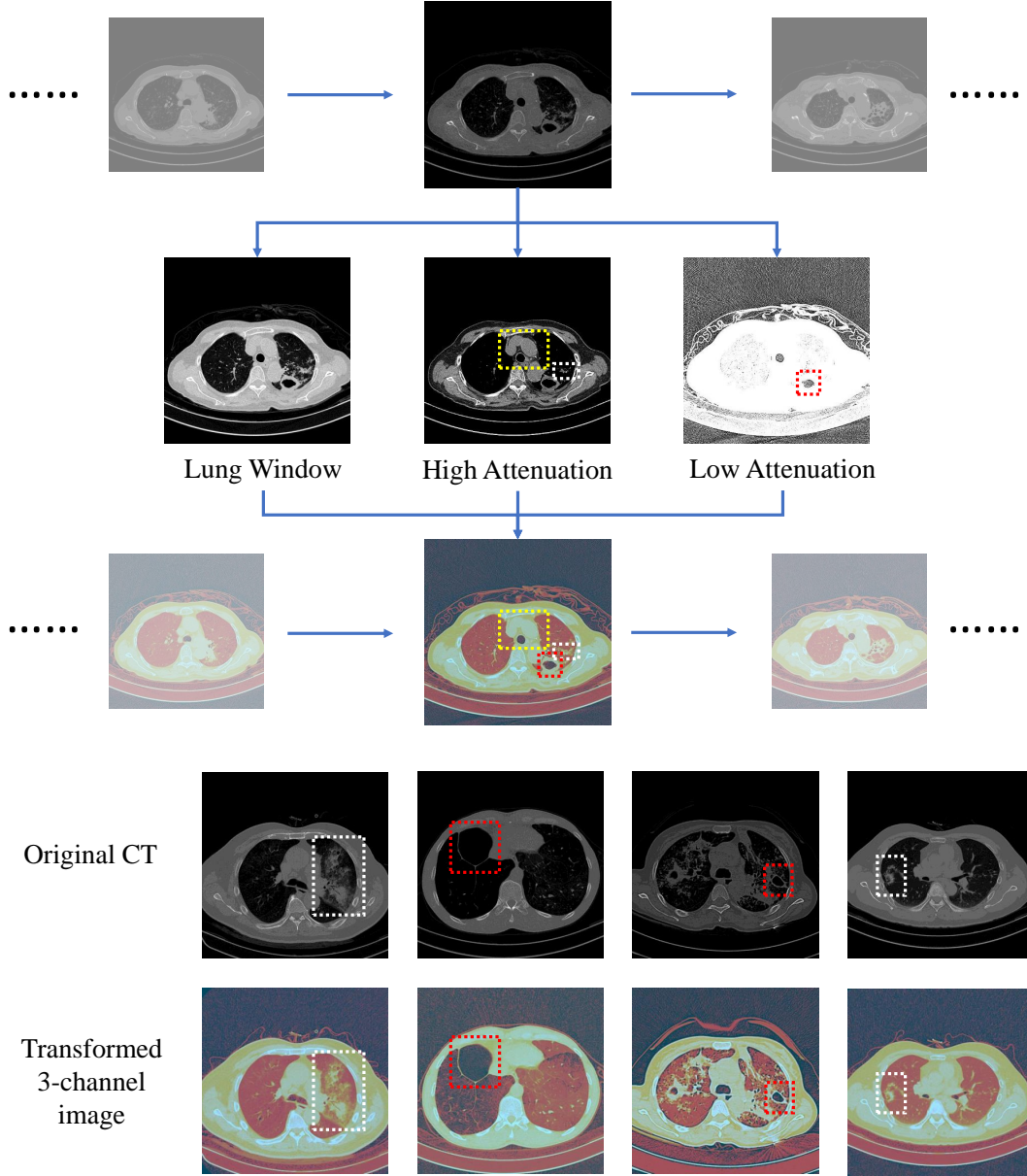


Fig. 4. Data Pre-process for CT Scans. Void space(in red rectangle) in original CT images is not very obvious since other normal tissues is in black color too. But in three-channel image, we can clearly notice the difference between normal tissues and low dense tissues. Moreover, the details of high dense tissues(in white rectangle) are still kept.

information at the same time. Follow the study [24], we use LSTM with 256 units as our RNN cells cause LSTM has been demonstrated to be capable of large-scale learning of sequence data.

We use CNN without fully-connected layers as feature extractor. The input size of CNN is 512×512 , so the outputs of CNN will be very large. We use global average pooling [29] to greatly reduce the number of neurons. It is a replacement of fully-connected layers to enable the summing of spatial information of feature maps. After global average pooling, we insert a fully-connected layer to reduce dimensions to 256 to fit the number of LSTM units. In order to get the best RCNN for CT scans, after LSTM layer, we insert two fully-

connected layers to give out classification results of RCNN, so that we can observe performances of different RCNNs and choose appropriate architecture. Experiments will be discussed later in section IV.

After building RCNN, we will keep architecture above LSTM(including LSTM) and insert into our MPDNet as encoder of visual features. It encodes image feature sequences and gives out the last output of LSTM as middle state hv_t :

$$hv_t = LSTM(Fx_t, hv_{t-1}, z_{t-1}) \quad (1)$$

Fx_t is the t -th visual features in CT slices, hv_{t-1} is LSTM hidden state of $t-1$ step, z_{t-1} is LSTM output of $t-1$ step. t is the length of slices, in this study, we set t as 32.

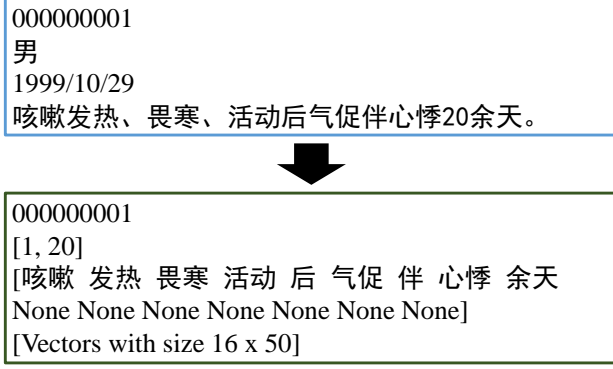


Fig. 5. Data Pre-process for Age, Gender and Chief Complaints

B. Multimodal Data Fusion

The whole RCNN, as mentioned in section III-A, can be seen as a encoder of CT images. Besides CT image information, we also have clinical information about patients gender, age, and chief complaints.

Details of processing steps have been discussed in section II-A2. The second LSTM is used to encode chief complaint. It is calculated in the same way as Eq. 1:

$$hc_{ct} = LSTM(Cx_{ct}, hc_{ct-1}, z_{ct-1}) \quad (2)$$

Cx_{ct} is word embedding matrix of the ct -th word in chief complaint, hc_{ct-1} is LSTM hidden state of $ct - 1$ step. ct is the length of chief complaint, which is 16.

After getting hv_t , hc_{ct} , we can calculate the prediction and loss Φ_1 as follows:

$$\Phi_1 = \sum_i y_i \log(\Delta_i),$$

$$\Delta = Softmax(F(hv_t \otimes hc_{ct} \otimes A \otimes G))$$

where y_i are vectors for labels, Δ is prediction after Softmax layer, \otimes is the concatenation operation, A is patient age, G is patient gender. F is a function to calculate joint distributions of hv_t , hc_{ct} , A and G . In this study, we use two fully-connected layers to fit the function. Φ_1 is cross-entropy that can be used as classification loss [26].

Since each case has 32 slices and calculate loss for only one time, we assume that the gradients propagate to CNN will be very weak, so that CNN will not be trained properly. Invoked by study in [30], we use a auxiliary loss to enhance signal of gradient for CNN. The auxiliary loss Φ_2 and loss of whole model $Loss$ are defined as follow:

$$Loss = (1 - \omega) \times \Phi_1 + \omega \times \Phi_2$$

$$\Phi_2 = \sum_i y_i \log(\Delta_i^c)$$

where ω is a parameter within the interval (0, 1). Φ_2 is classification cross-entropy loss from CNN, Δ_i^c is Softmax prediction of CNN. ω can adjust the weight of two losses at different training phases. We expect that at the beginning of training, CNN get stronger gradient and learn to capture features from CT images more quickly. After parameters of

CNN get stable, Φ_1 tends to get small and keep updating parameters of LSTM. Experiments also show that RCNN with auxiliary loss can have a better performance, which will be discussed latter in section IV. The parameters in MPDNet are optimized by minimizing the $Loss$.

Finally, MPDNet is built, RCNN for image data and LSTM for clinical information will be trained jointly.

IV. EXPERIMENTS

A. Experimental Setup

There are two steps in training process. The first step is to train different kinds of RCNN to get the best combination between CNN models and LSTM, the outputs from RCNN(1×256) will be feed into two fully connected layers to get classification results. We test performances of different LSTM units numbers (64, 128, 256, 512). Fig II shows that 64, 128 and 256 LSTM units have almost the same performances, they all get around 0.93 in accuracy, 512 LSTM units only get 0.915 in accuracy. As a result, we follow the study [24] and set the number of LSTM units 256.

TABLE II
PERFORMANCES OF DIFFERENT LSTM UNITS NUMBERS

Number of LSTM Units	Accuracy
64	0.930
128	0.935
256	0.930
512	0.915

Moreover, we use CNN models pre-trained on ImageNet [31]. Experiments show that using pre-trained models can significantly improve the converging speed, as shown in Table III. We can also prove the effect of three-channel images in this part of experiments.

TABLE III
COMPARISON BETWEEN TRAINING FROM SCRATCH AND TRAINING WITH PRE-TRAINED WEIGHTS

Structure	Pre-trained	Data	Accuracy
RCNN(ResNet)	No	LW Image	0.545
RCNN(GoogLeNet)	No	LW Image	0.545
RCNN(ResNet)	Yes	LW Image	0.925
RCNN(GoogLeNet)	Yes	LW Image	0.865

The second step is to train MPDNet model. We use RCNN as encoder for CT scan visual features, use LSTM as encoder for chief complaint features, and combine them with information of age and gender. All these features will be feed into two fully-connected layers and one Softmax layer to get final classification results. Initial learning rate is set to 0.0005 and drops 50% every 3000 training steps. The dropout rate in fully-connected layers is set to 0.5. MPDNet will be trained for 4 epoch, and each epoch contains 15 iteration for all training data. In this part of experiments, we will discuss the effect of chief complaints, age and gender.

B. Effect of Three-Channel Image

In order to verify the effect of three-channel image, we test three kinds of classic CNN models: VGG [32], ResNet [33] and GoogLeNet with Inception-V3 [30] with three-channel images, LW(Lung Window) images, HA(High Attenuation) images and LA(Low Attenuation) images. Experiment results are shown in Table IV. We can see that RCNN(VGG) and RCNN(ResNet) trained by Lung Window Image perform better in sensitivity, but their specificity are lower than 0.9. ResNet50 trained by three-channel image performs the best in accuracy, specificity, AUROC, so our RCNN use ResNet50 as its CNN part, and use one layer of LSTM cells as its RNN part. This conclusion is similar to [6], their experiments showed that ResNet50 outperformed GoogLeNet and VGG16.

Meanwhile, we output the feature maps of convolutional layer. Sample feature maps are shown in Fig 6. More specificity, we output the feature maps after one convolutional layer, one max pooling layer, and three ResNet blocks, the size of feature maps are 128×128 . In order to keep experiments environment consistent, all experiments carried on in this part are based on RCNN with ResNet50. We can see that CNN trained by three-channel images has advantages over CNNs trained by other kinds of images as shown in Fig 6. In Fig 6, images in the first column are original false color CT images, which are direct outputs from CT slices. The second, the third and the forth columns are feature maps from LW CNN, HA CNN and LA CNN. Images in the last column are feature maps from three-channel CNN. We can see that three-channel can keep both high dense information and low dense information.

C. Effect of Chief Complaints, Age and Gender

As mentioned in I, information about age, gender and chief complaints can enhance the features extracted from CT image or become a supplement. Chief complaints can provide information like symptoms, location. We count word frequency about symptoms. The frequency is shown in Table V and Table VI. We can see that top 10 key words in HC(healthy cases) and PC(pneumonic cases) have certain regularity. ‘Cough’ is the most frequent key word in both HC and PC. It appears 256 times(46.4%) in PC, 183 times(40.7%) in HC. However, symptoms like ‘Expectoration’, ‘Fever’, ‘Coughing blood’ appear more frequently in PC. For example, ‘Coughing blood’ appears 47 times in PC, but only appears 1 time in HC. Moreover, in Fig 7, according to the location and symptom information provided by chief complaints, we can accurately locate lesions in CT. It means information from chief complaints is related to CT images and can assist deep learning model.

D. Results

In order to prove the effect of auxiliary loss and multimodal data, we run a lot of experiments to compare with each other, and the results of experiments is shown in Table VIII.

We run an experiment to prove the effectiveness of auxiliary loss. We train RCNN(ResNet) with three channel image, but

we set ω to 1, which means we remove the gradient propagates directly to CNN, this model actually has only one loss. We can see that the performance of RCNN with single loss drops around 1% in all four indications. It proves that, by using auxiliary loss, CNN will be trained in a better way. We also output weights of two losses during training MPDNet, as shown in Table VII, weight for LSTM loss $(1 - \omega)$ is 0.6238 at the beginning of training (602 steps), however, $(1 - \omega)$ will increase to 0.7234 when training process comes to 36120 steps, it means weight for CNN is 0.3762 at 602 steps, and it will drop to 0.2766 at the end.

Then, we run experiments to prove that multimodal data can enhance the performance of CAD system. As shown in section 1, the output of RCNN, features of chief complaints, gender and age will be concatenated together and fused by two fully-connected layers. It is simple, but effective. We can see that MPDNet trained by multimodal data has the highest score in accuracy, specificity and AUROC score. But it achieves 0.936 in sensitivity, 0.009 lower than the highest 0.945. It means MPDNet has the best performance of binary classification according to its AUROC score. Besides, we remove the information about age and gender, we found that MPDNet without age and gender has a higher sensitivity and lower specificity than MPDNet with information about age and gender.

E. Discussion

If we treat RCNN(ResNet) trained with three-channel image as our baseline, we can see that complaint information can increase sensitivity with 1.8% to 94.5%, it means chief complaints do have information which can help to detect pneumonia. Meanwhile this information also decrease specificity to 90.1%, which is not hard to understand cause patients sometimes cannot accurately describe his feelings or even exaggerate his condition. If we add information about age and gender, the sensitivity drops a little bit, but the specificity increases to 95.6%, which means age and gender add information strongly connected to specificity.

The validation loss and accuracy during training is shown in Fig 8. We can see that MPDNet has the lowest loss and the highest accuracy during training. According to Fig 8, we can see that information about age and gender can improve accuracy to 0.7 at the very beginning, it means the dataset we are using must be influenced by some certain distribution. So we count the number of male patients and female patients in healthy cases and pneumonic cases(Table IX) and number of patients in different ages(Table X).

In Table IX, we can see that a male patient has a larger chance of getting pneumonia. In 601 male cases, about 60% of them are pneumonic, however, in 401 female cases, only 47.6% are pneumonic. This may be related to smoking since male in Chinese suffer a serious smoking problem. In Table X, we can see that age is also related to the chance of getting pneumonia. We can still observe that people older than 40 have much larger chance of getting pneumonia. There are about half of healthy cases between 40-50, but this indication drops so quickly that it goes down to 28.8% between 50-60. These two

TABLE IV
COMPARISON OF ALL KINDS OF RCNN

Structure	Data	Accuracy	Sensitivity	Specificity	AUROC
RCNN(VGG)	Lung Window Image	0.805	0.954	0.626	0.790
RCNN(GoogLeNet)	Lung Window Image	0.865	0.826	0.912	0.869
RCNN(ResNet)	Lung Window Image	0.925	0.954	0.890	0.922
RCNN(GoogLeNet)	High Attenuation Image	0.880	0.853	0.912	0.883
RCNN(ResNet)	High Attenuation Image	0.875	0.908	0.835	0.872
RCNN(GoogLeNet)	Low Attenuation Image	0.860	0.890	0.824	0.857
RCNN(ResNet)	Low Attenuation Image	0.865	0.900	0.824	0.861
RCNN(VGG)	Three Channel Image	0.890	0.927	0.846	0.886
RCNN(GoogLeNet)	Three Channel Image	0.905	0.900	0.912	0.906
RCNN(ResNet)	Three Channel Image	0.930	0.927	0.934	0.930

TABLE V
TOP 10 FREQUENT KEY WORDS IN PNEUMONIC CASES

Key Words	Frequency in PC	Percentage	Frequency in HC	Percentage
咳嗽, Cough	256	0.464	183	0.407
咳痰, Expectoration	103	0.187	42	0.093
反复, Repeat Condition	65	0.118	48	0.107
气促, Shortness of Breath	60	0.109	17	0.038
发热, Fever	51	0.092	14	0.031
咯血, Coughing Blood	47	0.085	1	0.002
加重, Aggravation	46	0.081	13	0.029
痰, Sputum	32	0.058	19	0.042
乏力, Weak	29	0.053	7	0.016
感染, Infection	28	0.051	1	0.002

Percentage is frequency divided by number of cases. PC is Pneumonic Cases. HC is Healthy Cases

TABLE VI
TOP 10 FREQUENT KEY WORDS IN HEALTHY CASES

Key Words	Frequency in HC	Percentage	Frequency in PC	Percentage
咳嗽, Cough,	183	0.407	256	0.464
胸痛, Chest Pain	67	0.149	17	0.031
不适, Uncomfortable	54	0.120	25	0.045
疼痛, Pain	53	0.118	25	0.045
反复, Repeat Condition	48	0.107	65	0.118
咳痰, Expectoration	42	0.093	103	0.187
背痛, Backache	28	0.062	8	0.014
痰, Sputum	19	0.042	32	0.058
胸闷, Chest Tightness	19	0.042	16	0.029
气促, Shortness of Breath	17	0.038	60	0.109

Percentage is frequency divided by number of cases. PC is Pneumonic Cases. HC is Healthy Cases

TABLE VII
WEIGHTS OF TWO LOSSES AT DIFFERENT TRAINING STEP

Number of Steps	$1 - \omega$	ω
602	0.6238	0.3762
9030	0.6547	0.3453
18060	0.7027	0.2973
27090	0.7185	0.2815
36120	0.7234	0.2766

tables explain why accuracy can achieve 0.7 at very beginning of training and why information about age and gender can improve specificity to 95.6%.

V. CONCLUSION

In this study, we propose a novel model MPDNet(Multimodal Pneumonia Detection Network), which combines CT visual features with patients' age, gender and chief complaints. In MPDNet, CT scans will be treated like video frames, and analyzed by RCNN(Recurrent Convolutional Neural Network), chief complaints will be transformed into word vectors by word2vec and analyzed by LSTM. Features from CT images and chief complaints will be fused together with patients' age and gender. All these features will be used to classify cases into healthy cases or pneumonic cases.

We analyze 1002 cases(450 healthy cases and 552 pneumonic cases). In fact, 1002 cases is far small than 'big data', so our model's performance is restricted by data distribution

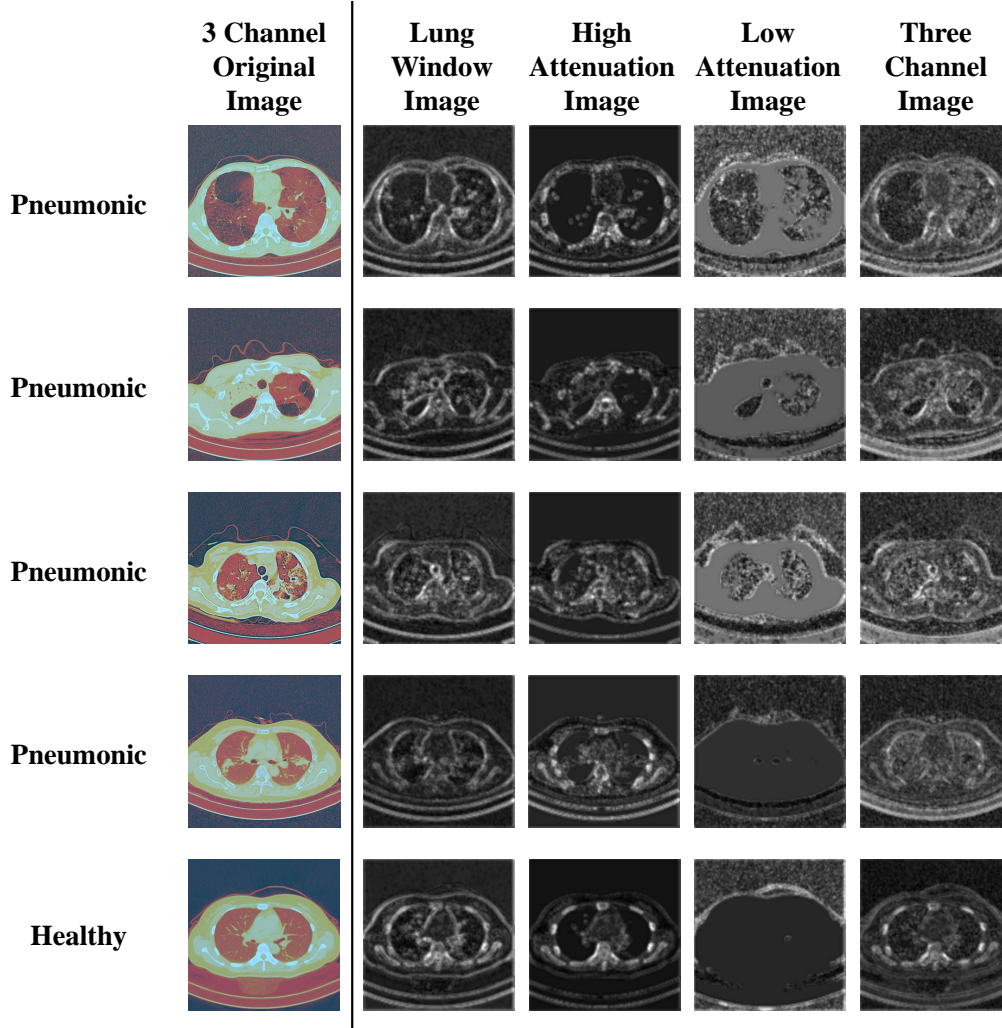


Fig. 6. Convolutional Feature Maps from CNN Models Trained by Different Images. In the first and the second rows, three-channel CNN can capture the low dense tissues of lungs, which are not very clear in LW(Lung Windows) CNN and HA(High Attenuation) CNN. LA(Low Attenuation) CNN can notice the low dense tissues, but apparently the details of heart and vessels are ignored in the low attenuation CNN. In the third and the fourth row, three-channel CNN still has ability to capture high dense tissues, which is the same as LW CNN and HA CNN, but LA CNN has difficulty in doing so. In the third row, LA CNN cannot distinguish the normal and abnormal tissues. Moreover, in the fourth row, LA CNN ignores high dense tissues. The last row shows a healthy case. Healthy case has a clear view in LW CNN, HA CNN and three-channel CNN, but shows nothing in LA CNN.

and quality. However, in clinical practice, it is very difficult to construct a big scale medical dataset for deep learning, cause raw data is affected by radiologists' personal habits, data acquisition equipments, and hospital work rules. Our future work will focus on methods which can overcome difficulties mentioned above. Moreover, our future work will also focus on diagnosing pneumonia like seasonal influenza virus pneumonia using more source of information, like medical history, family history, blood test and other information which will be considered during clinical practice. All works above will be carried out under the premise of respecting the privacy of the patients.

Source code for data pre-processing and MPDNet will be released very soon. We will also release model with trained parameters and some sample cases for demo. But we cannot release dataset because of the privacy of patients.

ACKNOWLEDGMENT

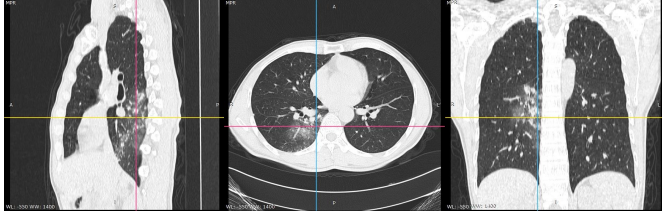
This work was partially supported by the National Natural Science Foundation of China (Grant no. 61772093), the Chongqing Major Thematic Projects (Grant no. cstc2018jzxcyztzxX0017). Xiaohong Zhang and Chen Liu are both the corresponding authors of the article.

REFERENCES

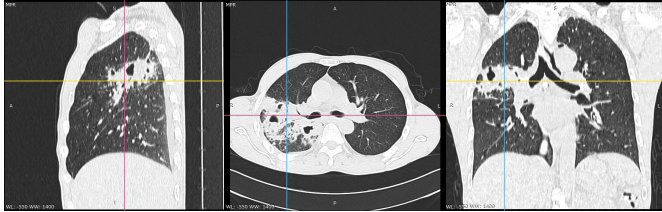
- [1] H. C. Shin, K. Roberts, L. Lu, D. Demner-Fushman, J. Yao, and R. M. Summers, "Learning to read chest x-rays: Recurrent neural cascade model for automated image annotation," in *Computer Vision & Pattern Recognition*, 2016.
- [2] N. Deepika, P. Vinupritha, and D. Kathirvelu, "Classification of lobar pneumonia by two different classifiers in lung ct images," in *2018 International Conference on Communication and Signal Processing (ICCSPP)*. IEEE, 2018, pp. 0552–0556.
- [3] D. K. Iakovidis, S. Tsevas, M. A. Savelonas, and G. Papamichalis, "Image analysis framework for infection monitoring," *IEEE Transactions on Biomedical Engineering*, vol. 59, no. 4, pp. 1135–1144, 2012.

TABLE VIII
COMPARISON OF ALL KINDS OF MPDNET

Structure	Data	Accuracy	Sensitivity	Specificity	AUROC	AUROC Rank
RCNN(ResNet)	Three Channel Image	0.930	0.927	0.934	0.930	2
RCNN(ResNet), One Loss	Three Channel Image	0.920	0.917	0.923	0.920	4
MPDNet	Three Channel Image & Complaints	0.925	0.945	0.901	0.923	3
MPDNet	Multimodal Data	0.945	0.936	0.956	0.945	1



院外检查右下肺阴影，伴咯血，7天。
Has been examined by another hospital, shadow in right lower lung, hemoptysis, 7 days.



反复咳嗽、咳痰伴右胸痛半年，加重1月。
Repeated cough, sputum, right chest pains for half a year, gets worse by one month.

Fig. 7. Chief complaints can provide information that related to CT images. In this figure, we show two cases which are pneumonic, each case has chief complaints provided by patients. Words marked red provide location, words marked blue provide symptoms. English chief complaints are translated from Chinese above. We can see that location and symptoms information provided by chief complaints are related to abnormal tissues in CT images.

TABLE IX
NUMBER OF MALE AND FEMALE PATIENTS IN HEALTHY AND PNEUMONIC CASES

	Healthy	Pneumonic	Total	Percentage*
Male	240	361	601	60.1%
Female	210	191	401	47.6%
Total	450	552	1002	55.1%

Percentage* is Percentage of Pneumonia Patients

- [4] S. Hochreiter and J. Schmidhuber, "Long short-term memory," *Neural Computation*, vol. 9, no. 8, pp. 1735–1780, 1997.
- [5] "Mesh: Medical subject headings," <https://www.nlm.nih.gov/mesh/meshhome.html>.
- [6] X. Wang, Y. Peng, L. Lu, Z. Lu, M. Bagheri, and R. M. Summers, "Chestx-ray8: Hospital-scale chest x-ray database and benchmarks on weakly-supervised classification and localization of common thorax diseases," *computer vision and pattern recognition*, pp. 3462–3471, 2017.
- [7] L. Yao, E. Poblentz, D. Dagunts, B. Covington, D. Bernard, and K. Lyman, "Learning to diagnose from scratch by exploiting dependencies among labels," *arXiv preprint arXiv:1710.10501*, 2017.
- [8] P. Rajpurkar, J. Irvin, K. Zhu, B. Yang, H. Mehta, T. Duan, D. Ding, A. Bagul, C. P. Langlotz, K. Shpanskaya *et al.*, "Chexnet: Radiologist-level pneumonia detection on chest x-rays with deep learning," *arXiv: Computer Vision and Pattern Recognition*, 2017.
- [9] X. Wang, Y. Peng, L. Le, Z. Lu, and R. M. Summers, "Tienet: Text-image embedding network for common thorax disease classification and reporting in chest x-rays," in *IEEE CVPR 2018*, 2018.

TABLE X
NUMBER OF HEALTHY AND PNEUMONIC CASES IN DIFFERENT AGES

	Healthy	Pneumonic	Total	Percentage*
0-10	6	1	7	14.3%
10-20	31	2	33	6.1%
20-30	122	30	152	19.7%
30-40	124	45	169	26.6%
40-50	109	108	217	49.8%
50-60	53	131	184	71.2%
60-70	5	126	131	96.2%
70-80	0	82	82	100%
> 90	0	27	27	100%
Total	450	552	1002	55.1%

Percentage* is Percentage of Pneumonia Patients

- [10] F. T, "Imaging of pneumonia: trends and algorithms," *European Respiratory Journal*, vol. 18, no. 1, pp. 196–208, 2001.
- [11] T. Cherian, E. K. Mulholland, J. B. Carlin, H. Ostensen, R. Amin, M. De Campo, D. Greenberg, R. Lagos, M. G. Lucero, S. A. Madhi *et al.*, "Standardized interpretation of paediatric chest radiographs for the diagnosis of pneumonia in epidemiological studies," *Bulletin of The World Health Organization*, vol. 83, no. 5, pp. 353–359, 2005.
- [12] P. D. Korfiatis, A. N. Karahaliou, A. D. Kazantzi, C. Kalogeropoulou, and L. I. Costaridou, "Texture-based identification and characterization of interstitial pneumonia patterns in lung multidetector ct," *IEEE Transactions on Information Technology in Biomedicine*, vol. 14, no. 3, pp. 675–680, 2009.
- [13] T. Yorozu, M. Hirano, K. Oka, and Y. Tagawa, "Electron spectroscopy studies on magneto-optical media and plastic substrate interface," *IEEE Translation Journal on Magnetism in Japan*, vol. 2, no. 8, pp. 740–741, 1987.
- [14] W. Hu, B. Cai, A. Zhang, V. D. Calhoun, and Y.-P. Wang, "Deep collaborative learning with application to multimodal brain development study," *IEEE Transactions on Biomedical Engineering*, 2019.
- [15] L. Xiao, J. M. Stephen, T. W. Wilson, V. D. Calhoun, and Y. Wang, "Alternating diffusion map based fusion of multimodal brain connectivity networks for iq prediction," *IEEE Transactions on Biomedical Engineering*, 2018.
- [16] Q. Dou, H. Chen, L. Yu, J. Qin, and P.-A. Heng, "Multilevel contextual 3-d cnns for false positive reduction in pulmonary nodule detection," *IEEE Transactions on Biomedical Engineering*, vol. 64, no. 7, pp. 1558–1567, 2016.
- [17] J. Wu, X. Liu, X. Zhang, Z. He, and P. Lv, "Master clinical medical knowledge at certificated-doctor-level with deep learning model," *Nature communications*, vol. 9, no. 1, p. 4352, 2018.
- [18] M. Xiaojian and W. Heyong, "Analysis of pathogens of pneumonia in children based on aprior algorithm," in *2011 IEEE International Symposium on IT in Medicine and Education*, vol. 1. IEEE, 2011, pp. 460–463.
- [19] J. S. Huang, Y. F. Chen, and J. C. Hsu, "Design of a clinical decision support model for predicting pneumonia readmission," in *2014 International Symposium on Computer, Consumer and Control*. IEEE, 2014, pp. 1179–1182.
- [20] H.-C. Shin, H. R. Roth, M. Gao, L. Lu, Z. Xu, I. Nogues, J. Yao, D. Mollura, and R. M. Summers, "Three aspects on using convolutional neural networks for computer-aided detection in medical imaging," in *Deep Learning and Convolutional Neural Networks for Medical Image Computing*. Springer, 2017, pp. 113–136.
- [21] M. Gao, U. Bagci, L. Lu, A. Wu, M. Buty, H.-C. Shin, H. Roth, G. Z. Papadakis, A. Depeursinge, R. M. Summers *et al.*, "Holistic classifi-

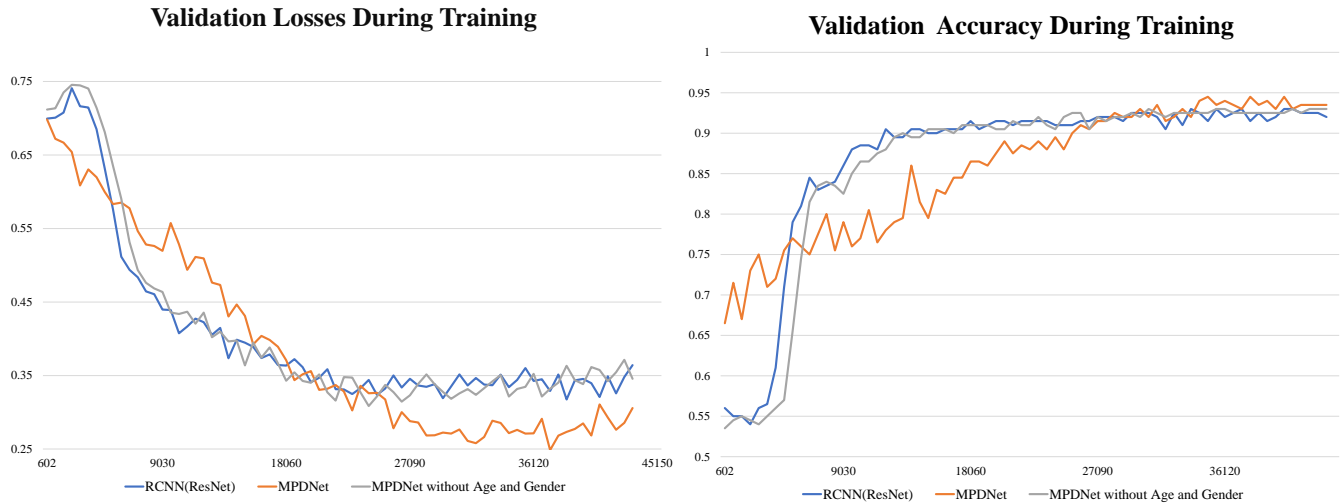
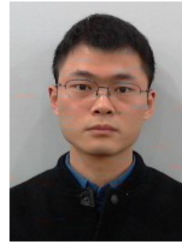


Fig. 8. Validation Loss and Accuracy During Training

cation of ct attenuation patterns for interstitial lung diseases via deep convolutional neural networks,” *Computer Methods in Biomechanics and Biomedical Engineering: Imaging & Visualization*, vol. 6, no. 1, pp. 1–6, 2018.

- [22] T. Mikolov, K. Chen, G. Corrado, and J. Dean, “Efficient estimation of word representations in vector space,” *arXiv preprint arXiv:1301.3781*, 2013.
- [23] T. Mikolov, I. Sutskever, K. Chen, G. S. Corrado, and J. Dean, “Distributed representations of words and phrases and their compositionality,” in *Advances in neural information processing systems*, 2013, pp. 3111–3119.
- [24] J. Donahue, L. Anne Hendricks, S. Guadarrama, M. Rohrbach, S. Venugopalan, K. Saenko, and T. Darrell, “Long-term recurrent convolutional networks for visual recognition and description,” in *Proceedings of the IEEE conference on computer vision and pattern recognition*, 2015, pp. 2625–2634.
- [25] N. Afaq, N. Akhtar, W. Liu, S. Z. Gilani, and A. Mian, “Spatio-temporal dynamics and semantic attribute enriched visual encoding for video captioning,” *arXiv preprint arXiv:1902.10322*, 2019.
- [26] M. Zreik, R. W. V. Hamersvelt, J. M. Wolterink, T. Leiner, and I. Isgum, “A recurrent cnn for automatic detection and classification of coronary artery plaque and stenosis in coronary ct angiography,” *IEEE Transactions on Medical Imaging*, vol. PP, no. 99, pp. 1–1, 2018.
- [27] J. Chung, C. Gulcehre, K. Cho, and Y. Bengio, “Empirical evaluation of gated recurrent neural networks on sequence modeling,” *arXiv preprint arXiv:1412.3555*, 2014.
- [28] K.-L. Tseng, Y.-L. Lin, W. Hsu, and C.-Y. Huang, “Joint sequence learning and cross-modality convolution for 3d biomedical segmentation,” in *Proceedings of the IEEE Conference on Computer Vision and Pattern Recognition*, 2017, pp. 6393–6400.
- [29] M. Lin, Q. Chen, and S. Yan, “Network in network,” *international conference on learning representations*, 2014.
- [30] C. Szegedy, V. Vanhoucke, S. Ioffe, J. Shlens, and Z. Wojna, “Rethinking the inception architecture for computer vision,” *computer vision and pattern recognition*, pp. 2818–2826, 2016.
- [31] O. Russakovsky, J. Deng, H. Su, J. Krause, S. Satheesh, S. Ma, Z. Huang, A. Karpathy, A. Khosla, M. Bernstein, A. C. Berg, and L. Fei-Fei, “ImageNet Large Scale Visual Recognition Challenge,” *International Journal of Computer Vision (IJCV)*, vol. 115, no. 3, pp. 211–252, 2015.
- [32] K. Simonyan and A. Zisserman, “Very deep convolutional networks for large-scale image recognition,” *international conference on learning representations*, 2015.
- [33] K. He, X. Zhang, S. Ren, and J. Sun, “Deep residual learning for image recognition,” *computer vision and pattern recognition*, pp. 770–778, 2016.



Qiuli Wang received the B.E. degree in the School of Information Engineering, Yangzhou University in 2016. He is currently working toward the Ph.D. degree in the School of Big Data & Software Engineering, Chongqing University.

His research interests include medical image computing, deep learning, so on.



Zhihuan Li received the B.E degree in Geological Engineering from China University of Mining and Technology, Xuzhou, China in 2016. He is currently working toward the M.S. degree in Software Engineering from the Department of Big Data & Software Engineering, Chongqing University, Chongqing. His research interests include medical image analysis, segmentation and so on.



Dan Yang received the B.Eng. degree in automation, the M.S. degree in applied mathematics, and the Ph.D. degree in machinery manufacturing and automation from Chongqing University, Chongqing. From 1997 to 1999, he held a post-doctoral position with the University of Electro-Communications, Tokyo, Japan. He is currently the President of Southwest Jiaotong University. He is also a Professor with the School of Big Data & Software Engineering, Chongqing University. He has authored over 100 scientific papers and some of them are published

in some authoritative journals and conferences, such as the IEEE TRANSACTIONS ON PATTERN ANALYSIS AND MACHINE INTELLIGENCE, CVPR, and BMVC. His research interests include computer vision, image processing, pattern recognition, software engineering, and scientific computing.



Chen Liu received the M.D. degree in Medical Imaging from Army Medical University, China, in 2015. He is currently an attending physicians in the Radiology Department of Southwest Hospital which is the first affiliated hospital of Army Medical University. He has hosted more than 6 research including National Natural Science Foundation and got funded more than 1.6 million. He published 6 articles as first author. His current research interests include brain functional MRI, clinical data mining, medical imaging deep learning.



Xiaohong Zhang received the M.S. degree in applied mathematics from Chongqing University, China, where he also received the Ph.D. degree in computer software and theory, in 2006. He is currently a Professor with the School of Big Data & Software Engineering, Chongqing University. His current research interests include data mining of software engineering, topic modeling, image semantic analysis, and video analysis.